Fluorescent Logic Systems for Sensing and Molecular Computation: Structure-Activity Relationships in Edge-Detection

ARTICLE TYPE

Fluorescent Logic Systems for Sensing and Molecular Computation: Structure-Activity Relationships in Edge-Detection

Jue Ling, Gaowa Naren, Jessica Kelly, Adam Qureshi and A. Prasanna de Silva

Received (in XXX, XXX) Xth XXXXXXXXX 20XX, Accepted Xth XXXXXXXXX 20XX
DOI: 10.1039/b000000x

Molecular logic-based computation continues to throw up new applications in sensing and switching, the newest of which is the edge detection of objects. The scope of this phenomenon is mapped out by the use of structure-activity relationships, where several structures of the molecules and of the objects are examined. The different angles and curvatures of the objects are followed with good-fidelity in the visualized edges, even when the objects are in reverse video.

Introduction

We established the generality of a molecular design tool – the fluorescent PET (photoinduced electron transfer) sensor/switch principle.[1-3] When this tool is used in an analogue mode, fluorescent molecular sensors arise. Some of these see service in clinics, hospitals, streets and war-zones all over the world in the measurement of blood electrolyte levels.[4,5] Related sensors also operate in veterinary contexts.[6] There is plenty of scope for the development of sensors in a similar manner for many more analytes in many other situations. When the above-mentioned tool is used in a digital mode, fluorescent molecular switches are produced.

These fluorescent switches form the vanguard of molecular logic[7]-based computation which is now engaging hundreds of laboratories worldwide. The results summarized in books[8-13] are augmented by those available in recent reviews[14,15] and articles.[16-27] This field offers tiny logical information processors that operate in biorelevant spaces which are too small for semiconductor devices to access conveniently.[28] This field also allows us to emulate deep-seated processes within ourselves which are molecular in nature.

Imagine the scene: a prehistoric hunter stalks the jungle looking to feed his family. The rustle of the undergrowth alerts him to an approaching animal. Will it be food or will he be food for it? Every millisecond counts. As soon as his retinas image the animal, his ganglion cells draw the edge of the animal as an outline. They send this highly-reduced dataset to his brain along the optic nerve and ask 'Do you recognize this outline?'. The brain replies 'This outline with its big ears, long nose and fat body matches that of an elephant on the warpath. Run!' and activates his legs. All of this happens within the millisecond-scale. The hunter escapes to hunt another day, rather than being trampled to a pulp. He was the common ancestor of you and me.

Just as edge detection saved the day for our hero long ago, it also looks after us on a daily basis[29,30] everytime any object approaches us at moderate speeds.[31] Edge detection is a deep-seated survival routine within us all. It is no surprise then that this routine has been adapted by computer scientists for security purposes, e.g. the rapid scanning of closed-circuit television footage, as well as for automation, e.g. the rapid inspection of mass-produced components for flaws.[32]

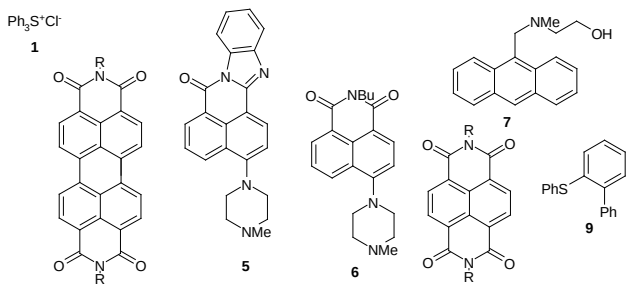

2; R = 2-[N,N-bis(2-hydroxyethyl)]aminoethyl
3; R = 2-(morpholino)ethyl
4; R = 2-(N,N-diethyl)aminoethyl

8; R = 2-(N,N-dimethyl)aminoethyl

More recently, edge detection was built-into bacteria by Ellington, Voigt and their team.[33] This was an important advance, even though the visualized edges were 0.4 cm thick at the thinnest. A follow-up paper by Ellington, Chen and co-workers[34] built edge detection into a reactive oligonucleotide network.[35] Excellent edge visualizations, 0.5 mm in width, were achieved provided that the matrix was precooled at 5 C and only warmed up to 37 C for the photographic observation. Furthermore, the observed edges blurred as time went by. We recently reported that small molecules, without any connotations or organizations of living systems, can detect edges under ambient conditions, resulting in edge widths of 1-2 mm which remain stable over considerable periods.[36] The extreme simplicity of the experiment was an added feature: a chemical-soaked and partially-dried filter paper is written and read with the two colours of a common laboratory ultraviolet lamp. The chemical composition required for the preparation of the filter paper was also simple: a photoacid generator, a H^+-driven fluorescent 'off-on' sensor and a Na_2CO_3 pH buffer.

The present work examines the range of applicability of this molecular computational effect, by considering a set of new results. These arise from a single photoacid generator, **1**,[37] and a range of fluorescent pH sensor structures **2**-**8**, all of which were available in our laboratory from our previous efforts concerning fluorescent PET sensors[2,38-41] and related sensors with TICT

(twisted internal charge transfer) excited states.[42-44] As maybe expected in an imaging experiment, the structure of the objects being imaged can also be varied so that insights into the phenomenon can be gained.

Results and Discussion

Molecular logical edge detection requires careful preparation of the filter paper by soaking it in a solution of **1**, **2** (say) and Na_2CO_3 in methanol:water (1:1, v/v) followed by drying in an oven at 50 C for 4 min. No drying resulted in very blurred images[36] and drying at 50 C for 10 min or longer resulted in clear positive photographs only.[36] These optimum conditions were developed for sensor **5**[36] and then, for convenience, used for all others without fresh optimization. Separate optimizations deserve to be done in future studies. The filter paper is then written with 254 nm light through a mask and read (after removing the mask) with 366 nm light excitation under our local conditions of temperature (ca. 20 C) and humidity (86 $\pm$ 5% annual average).

As seen in Figure 1, the fluorescence of **2** shows up clearly as an orange image in the time-lapse photographs. Initially, there is no orange fluorescence and only the blue background emission due to the filter paper and the components of the technical solution of **1** is seen. Then as the writing proceeds, the square object is imaged as an orange fluorescent square. We can recognize this as straightforward positive photography. Indeed, Tian's team previously observed this effect with **1** and a polymeric version of **6** following baking,[45] which is the common practice in industrial photolithography.[46] As the writing is continued, the orange fluorescent square image gains in intensity until 4 min and then undergoes a decline. This intensity decline is most apparent at the centre of the square and is virtually back to the background level at 32 min. This is fluorescence 'off-on-off' action driven by a light dose input.[47-50] In binary logic terms, this is XOR logic,[10,11] while it also has a ternary logic meaning.[11] However, the most visual aspect of the photograph at 32 min writing is that an orange fluorescence decorates the original edges of the square object. Edge detection in blue-green, in green and in orange were previously shown with sensors **5**, **6** and **3** respectively.[36]

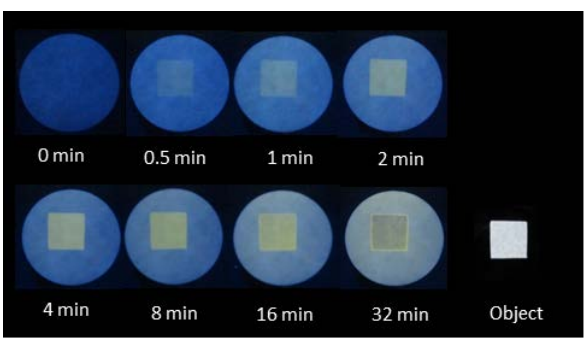

Figure 1. Photographs of fluorescent images after multiple exposure to writing light through the 'square' mask onto the substrate, containing the logical molecular solution including **2** prepared under optimum conditions, for varying cumulative times as noted in each photograph. Photograph of object under backlit conditions is also shown. For length calibration purposes, it is important to note the diameter of the filter paper to be 11.0 cm and the side of the square object to be 4.1 cm in all cases.

The working mechanism envisages H^+ produced by photolysis of **1** in the irradiated regions of the filter paper building up a concentration gradient at the edges between the irradiated and unirradiated regions. Diffusive movement of H^+ down this gradient produces neutralization of the pH buffer and switching 'on' of fluorescence of the sensor at the frontiers of the unirradiated regions. The fluorescence of the irradiated regions, which switch 'on' for the same reason at very early times, are gradually switched 'off' again due to the accumulation of the quencher **9** which acts bimolecularly. Occasionally, residual convective diffusion of H^+ contaminates the unirradiated regions to cause some enhancement of the background fluorescence.

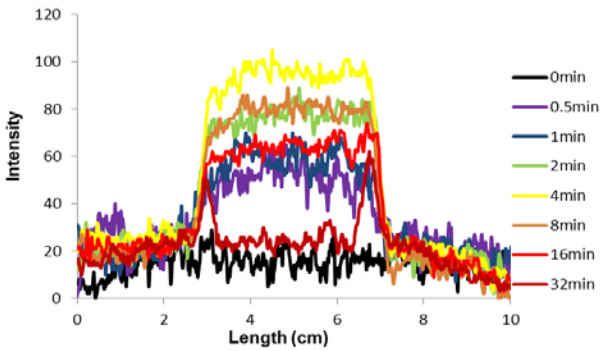

Figure 2. Intensity-length graphs of images in Figure 1 for a horizontal line through the centre of the square. For clarity, all graphs have been superimposed at the left foot.

This edge visualization can be quantitated by recourse to image analysis software commonly employed by microscopists. Fluorescence intensity – length graphs along a chosen line can be easily obtained in this manner. Figure 2 collects such data along a horizontal line through the centre of the square for each of the fluorescence photographs in Figure 1. The intensities are the red channel data following a red-green-blue analysis. The noisy nature of the graphs is partly due to the relatively weak intensities in this case and partly due to the roughness of the fibrous paper and subsequent drop in optical quality. However, the easy availability and inexpensiveness of the filter paper makes it the preferred matrix. The features of interest to us shine through the noise anyway. It can be noticed that the square expands slightly (ca. 1 mm) as the experiment proceeds. Most importantly, the scan at 32 min writing clearly shows a set of twin peaks, which are the visualized edges on the opposite sides of the square. The widths of these visualized edges are 0.27 (left) and 0.38 cm (right) respectively. These widths are somewhat expanded by repeated placement and removal of the mask which introduces errors in mask registration during multiple exposure experiments of this type.

Following the satisfactory edge detection by the logical molecular solution containing **2**, we carried out similar experiments with sensor **4** and the results are found in Figure 3. The edges of the square are not visualized with any clarity, and even the positive photograph stages do not show good contrast from the blue background. Our disappointment is tempered when we understand that sensor **4** is much less soluble in aqueous methanol than sensors **2** or **3**. Since it is difficult to get sufficient quantities of sensor **4** into the soaking solution, perhaps we should not be surprised at its failure to detect edges convincingly. Even the moderate hydrophilicity of the morpholino groups in **3** serve to counteract the propensity towards π-π stacking in these perylene compounds sufficiently for our purposes of edge detection. Sensors **6** and **7**, with their smaller π systems, have no such stacking worries.

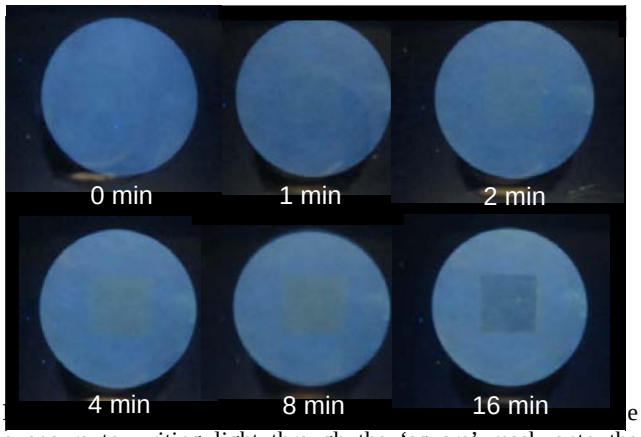

exposure to writing light through the 'square' mask onto the substrate, containing the logical molecular solution including **4** prepared under optimum conditions, for varying cumulative times as noted in each photograph.

In spite of the failure reported in the previous paragraph, we were in possession of several edge detecting systems in blue-green (with sensor **5**), in green (with sensor **6**) and in orange (with sensors **2** and **3**). So we went in search of a corresponding system which would signal in the blue range of the spectrum. Sensors **7**[41] and **8**[51] were evaluated. Figure 4 shows that molecular logic system containing **7** only shows negative photographs. No edges are visualized. Residual convective diffusion of H^+ most likely causes the bright blue emission in the unirradiated regions. Anthracene derivatives like **7** have intense absorptions around 254 nm due to S_0-S_2 transition with absorption coefficients (ε) of 10^5 M^{-1} cm^{-1}. So we have accidental overlap with the writing wavelength causing serious competitive absorption at the concentrations employed in our study. The photoacid generator **1**'s maximum ε is only $1.9x10^4$ M^{-1} cm^{-1} at 235 nm.[37] The non-emissive appearance of the irradiated region would suggest oxidative photodecomposition of **7** following direct excitation and subsequent PET to **1**. So the expected pathway for edge visualization is hijacked in this instance.

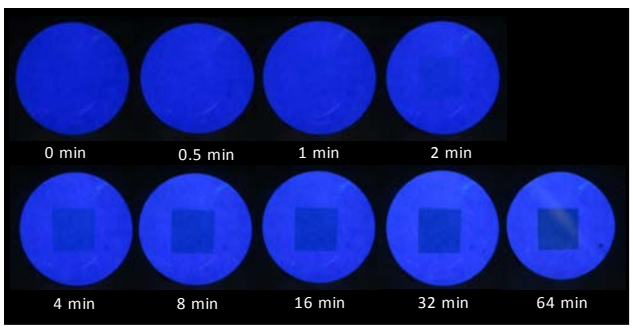

Figure 4. Photographs of fluorescent images after multiple exposure to writing light through the 'square' mask onto the substrate, containing the logical molecular solution including **7** prepared under optimum conditions, for varying cumulative times as noted in each photograph.

Similarly, Figure 5 shows no significant edge visualization for the case involving sensor **8**. Only a low-contrast negative photograph is seen. In this instance, the extremely electron-poor π-system of **8** and the electron-rich **9** pair up to cause strong quenching of emission in the irradiated region while residual convective diffusion of H^+ dominates the unirradiated regions and causes their emission. The search for edge visualization in blue goes on.

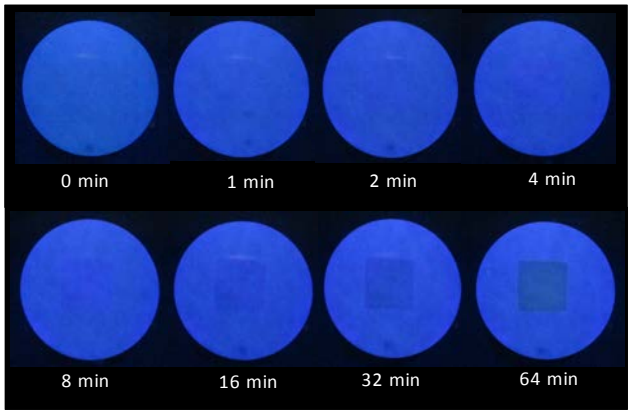

Figure 5. Photographs of fluorescent images after multiple exposure to writing light through the 'square' mask onto the substrate, containing the logical molecular solution including **8** prepared under optimum conditions, for varying cumulative times as noted in each photograph.

It was noted above that the current approach produces visualized edges that remain stable over time. This aspect is quantitated by writing through the object mask for the optimum time, followed by regular reading of the image while storing the filter paper in the dark under ambient conditions of temperature and humidity. The resulting images are collected in Figure 6. As we see, the visualized edges are well-preserved for 120 min in the cases of **6**, **3** and **2**. However, the visualized edges for **5** start to degrade after 30 min. Such stability over 30-120 min can be attributed to the progressive drying of the paper under ambient conditions so that H^+ (and other) diffusion ceases.

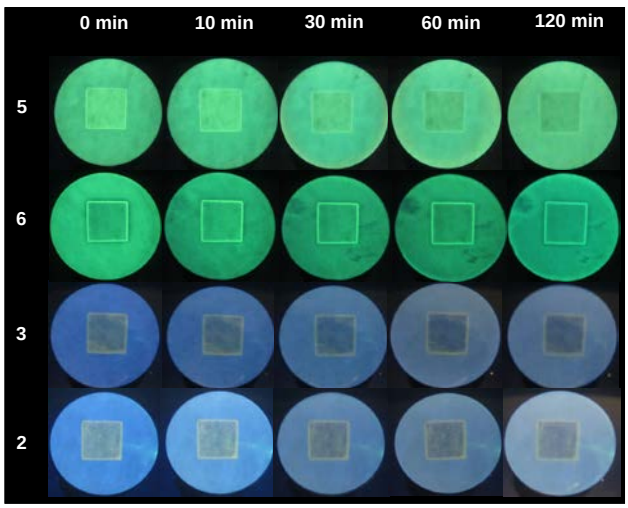

Figure 6. Photographs of fluorescent images after single exposure to writing light through the 'square' mask onto the substrate, containing the logical molecular solution including **5**, **6**, **3** and **2** prepared under optimum conditions, for 35, 16, 35 and 35 min respectively, after standing in the dark for varying cumulative times as noted above each column.

The object has been a hole cut in an opaque mask upto now. Reversal of this situation is important to examine. In the early

days of mainframe computers, dumb terminals followed the trend in mechanical typewriters and could only display plain text characters in a single colour, font and fontsize. One way to introduce some variety was to reverse the illumination of the character. Then the reverse-video character would have more lit pixels than dark ones. To emulate this, we lay the object (cut from opaque and rigid material) directly on the prepared filter paper prior to writing. Now, the irradiated regions are larger in area than their unirradiated counterparts, so that more protons would be generated than in previous experiments. Then, residual convective diffusion of H^+ could be a bigger nuisance, for instance. In order to mitigate such an effect to some extent, we lay down an arbitrary combination of differently-shaped objects. Such combinations also offer insight into potential interference between diffusing proton fronts where two objects are rather close to each other in space.

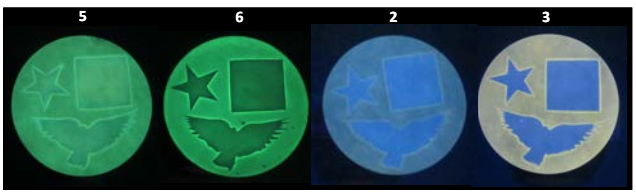

Figure 7. Photographs of fluorescent images after single exposure to writing light through a combination of opaque 'square', 'star' and 'bird' masks onto the substrate, containing the logical molecular solution including **5**, **6**, **3** and **2** prepared under optimum conditions, for 35, 16, 35 and 35 min respectively. The square is 4.1 cm side.

Gratifyingly, clear edge visualization occurs in all four cases (Figure 7). No interference effects are seen. The low backgrounds in the unirradiated regions in the cases of systems involving **6**, **2** and **3** are to be noted, whereas the case involving **5** does show some residual convective diffusion of H^+ into the unirradiated regions which leads to some fluorescence enhancement. Therefore the contrast of the visualized edge in the case of **5** is noticeably smaller than those seen with sensors **6** and **3**. The contrast of the visualized edge with **2** is also small because of its solubility limitations. Some quantitative analysis was made by obtaining fluorescence intensity - length graphs along a line through the centre of the square and parallel to a quasi-horizontal side. Green (for **5** and **6**) and red (for **2** and **3**) channel data are employed. These graphs (Figure 8) allow the estimation of the widths of the visualized edges to be 0.8 - 1.8 mm.

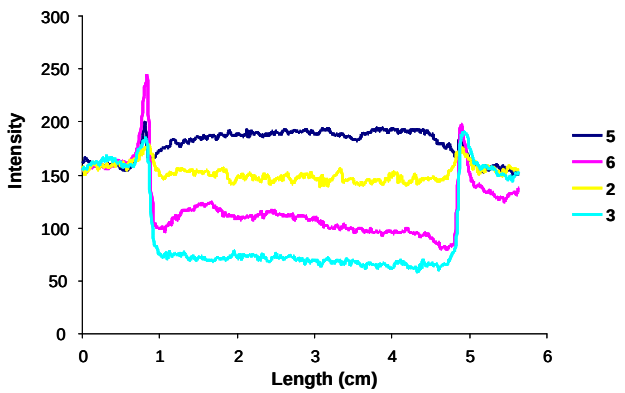

Figure 8. Intensity-length graphs of 'square' images only in Figure 7 for a line through the centre of the square and parallel to a quasi-horizontal side. For clarity, all graphs have been superimposed at the left foot.

Conclusion

Structure-activity relationships in edge-detecting molecular logic systems help to delineate the scope of this new phenomenon in molecular computation. A general mechanism emerges, which is based on photoproduction of protons in written regions, followed by slow diffusive encroachment across the boundaries into unwritten regions. Proton-induced switching 'on' of fluorescence then occurs in these areas. Subsequent erasure of the fluorescence takes place in the irradiated areas as a product gradually accumulates and asserts itself as a bimolecular quencher. 'Off-on-off' fluorescence[41,52-54,23] driven by light dose is therefore crucial to the success of these experiments. Some sensors fail at edge detection because of competitive absorption of the writing light. However this is not fatal since writing light sources other than the humble mercury arc lamp are available for future exploitation. Other sensors fail due to excessive quenching. Yet others fail due to inadequate solubility. However, a good number of easily-synthesized sensors succeed at achieving this human-level computation under very simple conditions.

We thank DEL Northern Ireland, X. G. Ling and L. H. Wang for support and help.

Notes and references

Address, School of Chemistry and Chemical Engineering, Queen's University, Belfast BT9 5AG, Northern Ireland. Tel: (+)44 28 9097 4422; Fax: (+)44 28 9097 4687; E-mail: a.desilva@qub.ac.uk

1 A. J. Bryan, A. P. de Silva, S. A. de Silva, R. A. D. D. Rupasinghe and K. R. A. S. Sandanayake, *Biosensors* 1989, **4**, 169.
2 A. P. de Silva, H. Q. N. Gunaratne, T. Gunnlaugsson, A. J. M. Huxley, C. P. McCoy, J. T. Rademacher and T. E. Rice, *Chem. Rev.* 1997, **97**, 1515.
3 A. P. de Silva, T. S. Moody and G. D. Wright, *Analyst* 2009, **134**, 2385.
4. J. K. Tusa and H. He, *J. Mater. Chem.* 2005, **15**, 2640.
5 www.optimedical.com.
6 www.idexx.com.
7 A. P. de Silva, H. Q. N. Gunaratne and C. P. McCoy, *Nature* 1993, **364**, 42.
8 *Molecular and Supramolecular Information Processing*, (Ed: E. Katz), Wiley-VCH, Weinheim, 2012.
9 *Biomolecular Information Processing*, (Ed: E. Katz), Wiley-VCH, Weinheim, 2012.
10 K. Szacilowski, *Infochemistry*, Wiley, Chichester, 2012.
11 A. P. de Silva, *Molecular Logic-based Computation*, Royal Society of Chemistry, Cambridge, 2013.
12 V. Balzani, A. Credi and M. Venturi, *Molecular Devices and Machines. 2nd Ed.* VCH, Weinheim, 2008.
13 *Molecular Switches. 2nd Ed.* (Eds. B. L. Feringa and W. R. Browne) Wiley-VCH, Weinheim, 2011.
14 J. Andreasson and U. Pischel, *Chem. Soc. Rev.* 2015, **44**, 1053.
15 B. Daly, J. Ling, V. A. Silverson and A. P. de Silva, *Chem. Commun.* 2015, **51**, DOI: 10.1039/c4cc10000j.
16 M. Isjk, R. Guliyev, S. Kolemen, Y. Altay, B. Senturk, T. Tekinay and E. U. Akkaya, *Org. Lett.* 2014, **16**, 3260.
17 E. T. Ecik, A. Atilgan, R. Guliyev, T. B. Uyar, A. Gumus and E. U. Akkaya, *Dalton Trans*. 2014, **43**, 67.
18 S. Erbas-Cakmak and E. U. Akkaya, *Angew. Chem. Int. Ed.* 2013, **52**, 11364.
19 M. Warzecha, M. Oszajca, K. Pilarczyk and K. Szacilowski, *Chem. Commun.* 2015, **51**, 3559.
20 T. J. Farrugia and D. C. Magri, *New J. Chem*. 2013, **37**, 148.
21 D. C. Magri, M. Camilleri Fava and C. J. Mallia, *Chem. Commun.* 2014, **50**, 1009.

22 M. V. Caruana, M. Camilleri Fava and D. C. Magri, *Asian J. Org. Chem.* 2015, **4**, 239.
23 R. Zammit, M. Pappova, E. Zammit, J. Gabarretta and D. C. Magri, *Canad. J. Chem*. 2015, **93**, 199.
24 B. Rout, L. Unger, G. Armony, M. A. Iron and D. Margulies, *Angew. Chem. Int. Ed.* 2012, **124**, 12645.
25 B. Rout, P. Milko, M. A. Iron, L. Motiei and D. Margulies, *J. Am. Chem. Soc*. 2013, **135**, 15330.
26 B. Rout, L. Motiei and D. Margulies, *Synlett* 2014, **25**, 1050.
27 M. Elstner, J. Axthelm and A. Schiller, *Angew. Chem. Int. Ed*. 2014, **53**, 7339.
28 A. P. de Silva, M. R. James, B. O. F. McKinney, D. A. Pears and S. M. Weir, *Nature Mater.* 2006, **5**, 787.
29 V. Bruce, P. R. Green and M. A. Georgeson, *Visual Perception 4th Ed*. Psychology Press, Hove, 2003.
30 *How animals see the world*, (Eds. O. F. Lazareva, T. Shimizu and E. A. Wasserman), Oxford University Press, Oxford, 2012.
31 S. H. Hock and D. F. Nichols, *Atten. Percept. Psychophys.* 2013, **75**, 726.
32 L. G. Shapiro and G. C. Stockman, *Computer Vision*, Prentice-Hall, Upper Saddle River, NJ, 2001.
33 J. J. Tabor, H. M. Salis, Z. B. Simpson, A. A. Chevalier, A. Levskaya, E. M. Marcotte, C. A. Voigt and A. D. Ellington, *Cell* 2009, **137**, 1272.
34 S. M. Chirieleison, P. B. Allen, Z. B. Simpson, A. D. Ellington and X. Chen, *Nature Chem*. 2013, **5**, 1000.
35 N. Wagner and G. Ashkenasy, *Chem. Eur. J*. 2009, **15**, 1765.
36 J. Ling, G. W. Naren, J. Kelly, T. S. Moody and A. P. de Silva, *J. Am. Chem. Soc.* 2015, **137**, 3763.
37 J. L. Dektar and N. P. Hacker, *J. Am. Chem. Soc.* 1990, **112**, 6004.
38 L. M. Daffy, A. P. de Silva, H. Q. N. Gunaratne, C. Huber, P. L. M. Lynch, T. Werner and O. S. Wolfbeis, *Chem. Eur. J*. 1998, **4**, 1810.
39 A. P. de Silva and S. Uchiyama, *Top. Curr. Chem.* 2011, **300**, 1.
40 B. Daly, J. Ling and A. P. de Silva, *Chem. Soc. Rev.* 2015, **44**, DOI: 10.1039/c4cs00334a
41 A. P. de Silva, H. Q. N. Gunaratne and C. P. McCoy, *Chem. Commun.* 1996, 2399.
42 S. Zheng, T. S. Moody, P. L. M. Lynch, H. Q. N. Gunaratne, T. E. Rice and A. P. de Silva, *Photochem. Photobiol. Sci.* 2012, **11**, 1675.
43 W. Rettig, *Top. Curr. Chem*. 1994, **169**, 253.
44 Z. R. Grabowski and J. Dobkowski, *Pure Appl. Chem*. 1983, **55**, 245.
45 H. Tian, J. Gan, K. C. Chen, J. He, Q. L. Song and X. Y. Hou, *J. Mater. Chem.* 2002, **12**, 1262.
46 J. S. Kilby, *ChemPhysChem*, 2001, **2**, 482.
47 F. Pina, M. J. Melo, M. Maestri, P. Passaniti and V. Balzani, *J. Am. Chem. Soc*. 2000, **122**, 4496.
48 S. Silvi, E. C. Constable, C. E. Housecroft, J. E. Beves, E. L. Dunphy, M. Tomasulo, F. M. Raymo and A. Credi, *Chem. Commun*. 2009, 1484.
49 S. Silvi, E. C. Constable, C. E. Housecroft, J. E. Beves, E. L. Dunphy, M. Tomasulo, F. M. Raymo and A. Credi, *Chem. Eur. J.* 2009, **15**, 178.
50 M. P. O'Neil, M. P. Niemczyk, W. A. Svec, D. Gosztola, G. L. Gaines III and M. R. Wasielewski, *Science* 1992, **257**, 63.
51 M. S. Refat, I. Grabchev, J. -M. Chovelon and G. Ivanova, *Spectrochim. Acta A* 2006, **64**, 435.
52 S. A. de Silva, A. Zavaleta, D. E. Baron, O. Allam, E. V. Isidor, N. Kashimura and J. M. Percarpio, *Tetrahedron Lett*. 1997, **38**, 2237.
53 Y. Diaz-Fernandez, F. Foti, C. Mangano, P. Pallavicini, S. Patroni, A. Gramatges and S. Rodriguez-Calvo, *Chem. Eur. J.* 2006, **12**, 921.
54 V. F. Pais, P. Remon, D. Collado, J. Andreasson, E. Perez-Inestrosa and U. Pischel, *Org. Lett*. 2011, **13**, 5572.

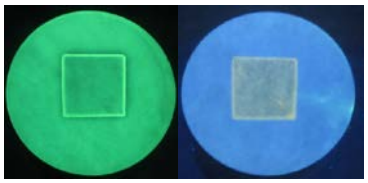

Table of Contents Entry

Several fluorescent 'off-on' sensors can be combined with a photoacid generator and a pH buffer on filter paper to yield edge detecting logic systems which operate on objects of different structures.

Table of Contents Graphic